Journal of Theoretical Biology 386 (2015) 122–131

Contents lists available at ScienceDirect

Journal of Theoretical Biology

journal homepage: www.elsevier.com/locate/yjtbi

Physical and computational fluid dynamics models for the hemodynamics of the artiodactyl carotid rete

Haley D. O'Brien *, Jason Bourke

Ohio University Department of Biological Sciences, 107 Irvine Hall, Athens, OH 45701, United States

HIGHLIGHTS

- Multiple physical models demonstrate that the artiodactyl carotid rete is structurally incapable of mitigating cerebral blood pressure.
- Computational models indicate a reduction in rates of blood flow within the branches of the carotid rete, potentially facilitating heat exchange.
- Artiodactyls, especially those with elongate necks, are likely employing alternative hemodynamic mechanisms to mitigate extreme changes in cranial blood pressure.

GRAPHICAL ABSTRACT

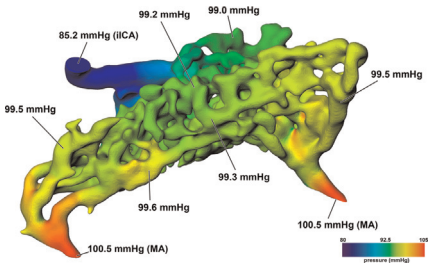

ARTICLE INFO

Article history:
Received 23 February 2015
Received in revised form
9 September 2015
Accepted 11 September 2015
Available online 25 September 2015

Keywords:
Carotid rete
Computational fluid dynamics
Hagen–Poiseuille's equation
Hemodynamics
Artiodactyla

ABSTRACT

In the mammalian order Artiodactyla, the majority of arterial blood entering the intracranial cavity is supplied by a large arterial meshwork called the carotid rete. This vascular structure functionally replaces the internal carotid artery. Extensive experimentation has demonstrated that the artiodactyl carotid rete drives one of the most effective selective brain cooling mechanisms among terrestrial vertebrates. Less well understood is the impact that the unique morphology of the carotid rete may have on the hemodynamics of blood flow to the cerebrum. It has been hypothesized that, relative to the tubular internal carotid arteries of most other vertebrates, the highly convoluted morphology of the carotid rete may increase resistance to flow during extreme changes in cerebral blood pressure, essentially protecting the brain by acting as a resistor. We test this hypothesis by employing simple and complex physical models to a 3D surface rendering of the carotid rete of the domestic goat, *Capra hircus*. First, we modeled the potential for increased resistance across the carotid rete using an electrical circuit analog. The extensive branching of the rete equates to a parallel circuit that is bound in series by single tubular arteries, both upstream and downstream. This method calculated a near-zero increase in resistance across the rete. Because basic equations do not incorporate drag, shear–stress, and turbulence, we used computational fluid dynamics to simulate the impact of these computationally intensive factors on resistance. Ultimately, both simple and complex models demonstrated negligible changes in resistance and blood pressure across the arterial meshwork. We further tested the resistive potential of the carotid rete by simulating blood pressures known to occur in giraffes. Based on these models, we found resistance (and blood pressure mitigation as a whole) to be an unlikely function for the artiodactyl carotid rete.

* Corresponding author. Present address: Department of Anatomy and Cell Biology, Oklahoma State University Center for Health Sciences, 1111 West 17th Street, Tulsa, OK 74107, United States. Tel.: +1 740 593 2290.
E-mail addresses: Haley.OBrien@okstate.edu (H.D. O'Brien), Jason.Bourke.1@ohio.edu (J. Bourke).

http://dx.doi.org/10.1016/j.jtbi.2015.09.008
0022-5193/

1. Introduction

The mammalian order Artiodactyla includes all even-toed ("cloven hoofed") ungulates. As the most prolific group of extant ungulates, artiodactyls possess a number of unique morphological and physiological specializations thought to augment their evolutionary success relative to other hoofed mammals (Janis, 1976, 1989, 2007, 2008; Kohler, 1993; Jernvall et al., 1996; Janis et al., 1998; Kohler and Moya-Sola, 2001; Mitchell and Lust, 2008). One such specialization is the carotid rete, an extensive subdural cranial arterial meshwork that supplies the majority of blood to the brain and meninges. This structure functionally, and sometimes completely, replaces the internal carotid artery during development (Daniel et al., 1953; Gillilan, 1974; Wible, 1984), resulting in a cranial vascular pattern that is unique to artiodactyls among mammals (Sisson and Grossman, 1967); Fig. 1. Although other mammals possess a carotid rete, including domestic cats (Hayward and Baker, 1969), lorisiform primates (Kanagasuntheram and Krishnamurti, 1965), and perhaps elephants (Shoshani et al., 2006), none rival the elaborate rete of artiodactyls, and none are fully enclosed by the cavernous venous sinus. This exceptional morphology may impart a variety of functions that are exclusive to artiodactyls.

The most thoroughly investigated function of the carotid rete is its role as a vital component of selective brain cooling (reviewed in Caputa, 2004). The carotid rete is situated within the cavernous sinus, which receives venous tributaries from the anterior cerebrum and meninges, as well as from anterior facial veins that drain the evaporatively-cooled nasal mucosa of the maxilloturbinates (Negus, 1958). The blood received by the cavernous sinus is therefore significantly cooler than the animal's body temperature. The high surface area of the arterial meshwork then allows rapid heat dissipation from the blood bound for the brain and into the excurrent venous system (Baker and Hayward, 1967; Hayward and Baker, 1969; Taylor, 1970; Mitchell et al., 1987). This coupling results in one of the most effective mechanisms of brain cooling recorded for terrestrial vertebrates (Caputa, 2004). Many functional and experimental studies confirm the rete's role in thermoregulatory physiology across aerobic exercise (Taylor and Lyman, 1972; Jessen, 1998) and while free-ranging (Jessen et al., 1994; Fuller et al., 1999; Maloney et al., 2002; Lust et al., 2007). The cooling effect on the brain, particularly the hypothalamus, delays panting and sweating, compounding the temperature decline with a reduction in evaporative water loss (Taylor, 1970; Taylor and Lyman, 1972; Robertshaw and Demi'el, 1983; Kuhnen, 1997; Aas-Hansen et al., 2000; Robertshaw, 2006). It is clear that the carotid rete plays an extensive role in artiodactyl homeostasis. Less clear is the impact this mesh-like structure may have on the hemodynamics of cerebral circulation and perfusion (Miletich et al., 1975; Mitchell et al., 2008). Questions remain unanswered regarding how replacement of a single internal carotid artery with a large rete would impact blood flow to the brain.

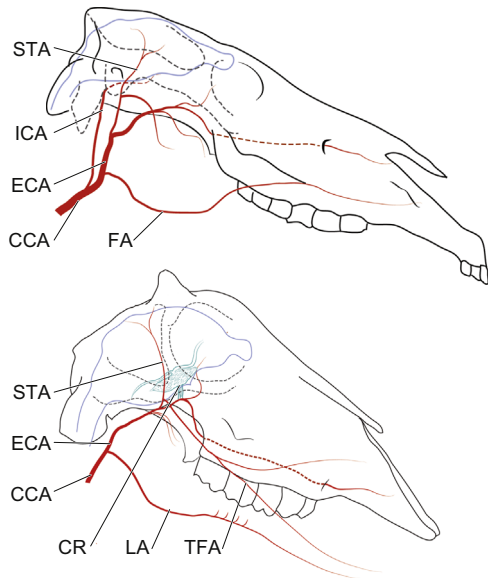

Fig. 1. Cranial arterial schematic of (a) the domestic horse (Equus ferus caballus) and (b) a domestic goat (Capra hircus hircus). The distributing arteries of the horse follow a more typical mammalian pattern, with a common carotid artery (CCA) that terminates as internal and external carotid arteries (ICA and ECA, respectively). Artiodactyls, as represented by the goat, generally do not possess an ICA, instead supplying the intracranial cavity *via* the carotid rete (CR; in teal). Abbreviations: CCA, common carotid artery; CR, carotid rete; ECA, external carotid artery; FA, facial artery; ICA, internal carotid artery; LA, lingual artery; STA, superficial temporal artery; TFA, transverse facial artery.

The question of whether such a structure initiates changes in blood pressure is particularly relevant to artiodactyls, many of which, such as goats, gerenuks, alpacas, llamas, camels, and giraffes, have relatively long necks for their body size. For these animals, the simple act of lifting or lowering their heads can dramatically raise or decrease cranial blood pressure. In the giraffe (*Giraffa camelopardalis*), for example, the neurocranium is an average of 2.07 m from the heart. When the head is lowered to the ground, it passes through a 3.5-m change in elevation. Due to the effects of gravity and positioning the head below the level of the heart, there are drastic and rapid changes in blood pressure at the head. When the animal assumes a natural posture, with its head up, the average cranial blood pressure is 145/55 mmHg (systole/diastole); with its head down, cranial blood pressure is approximately 330/240 mmHg (van Citters et al., 1968, 1969; Hargens et al., 1987). For comparison, in the human brain, a systolic blood pressure of 160 or higher is considered high risk for stroke and aneurysm (Goetz, 1955; Klabunde, 2005; Moore et al., 2010). When the giraffe raises its head again, pressure suddenly drops. Without an intervening physiological mechanism, the animal should faint (Patterson et al., 1957; van Citters et al., 1968, 1969; Mitchell and Skinner, 1993; Mitchell et al., 2008), especially since the heart is incapable of raising pulse rate high enough to accommodate this loss of pressure (Goetz, 1955). Obviously the animal does not faint, but few attempts have been made to quantify the hemodynamics alleviating cranial pressure changes. It has been hypothesized that the carotid rete may be a mechanism for mitigating these rapid changes in blood pressure. There are two potential mechanisms for cerebral blood pressure control, including: 1) contraction to block the rush of blood (Ask-Upmark, 1935; Edelman et al., 1972; van Citters et al., 1969); or 2) expansion to absorb sudden excess blood volume (Edelman et al., 1972). Essentially, the carotid rete may act in a manner analogous to an electrical capacitor. Although the giraffe is an extreme example, other long-necked animals should experience similar, albeit lower magnitude changes in cerebral arterial pressure across head raising and lowering.

Here we model potential changes in resistance, blood pressure, and shear stress to test the hypothesis that the artiodactyl carotid rete plays a role in regulation of cerebral perfusion. Since arterial morphology is relatively conserved among ruminant artiodactyls, especially in relation to the vessels supplying the carotid rete (Lawrence and Rewell, 1948; Daniel et al., 1953; Carlton and McKean, 1977), we used the domestic goat, *Capra hircus* as an anatomical model. Although goats do not represent the extreme of artiodactyl neck length, their use as a medical model has yielded a wealth of information on their blood properties (including blood volume, density, viscosity, hematocrit, pressure, and flow rates). These values are vital components of this investigation and are infrequently available for the relevant non-domesticated taxa. We model the capacity of the rete to adjust resistance to flow using two methods: 1) a basic hemodynamic approach, and 2) a more

complex computational fluid dynamics (CFD) model. In our basic approach, we estimate fluid flow mechanics by modeling systemic hemodynamics using similar equations as those used to model electrical circuits. Single arteries of different diameters within an arterial tree are compiled as "wires" of different resistance values that have been arranged in series, whereas arterial networks are modeled as wires in parallel. When properties of resistance or flow across parallel circuits are calculated, the results can then be inserted additively within the series of more discrete vessels. The CFD model utilized more complex algorithms that account for additional parameters that would be relevant to biological systems, such as the drag imposed by arterial walls and the potential turbulence created by multiple bifurcations. Ultimately, both simple and complex models indicate that resistance to flow across the rete (and therefore change in blood pressure) is effectively zero. These results suggest that the structure of the carotid rete itself is hemodynamically equivalent to a normal internal carotid artery.

2. Materials and methods

2.1. Anatomical data collection

Anatomical data collection involved radiopaque latex vascular injection of a single specimen of domestic goat (*Capra hircus*), followed by CT scanning and digital segmentation to appropriately assess carotid rete segmentation and to generate a digital surface for CFD. This animal was part of an in-house study unrelated to this research, and died of natural causes. No animals were sacrificed for the purpose of this study, and no institutional permissions were required for the use of cadaveric specimens. Shortly after the time of death, the goat was exsanguinated and frozen to prevent tissue necrosis and blood coagulation.

Specimen preparation followed O'Brien and Williams (2014). After being thoroughly thawed, the common carotid arteries were isolated in dissection. Small diameter 1/16th inch medical-grade PVC tubing (Thermo Scientific Nalgene) was inserted into the right common carotid artery and secured with hemostats, surgical ligature, and adhesive. The arterial system was flushed with water for 10 min, followed by a second flush with 90 mL of 10% One-Point anticoagulant solution. The specimen was then injected with a solution of 40% Liquid Polibar Plus barium sulfate suspension (BaSO4, E-Z-Em, Westbury, NY) in red liquid latex injection medium (Ward's, Rochester, NY). This ratio of radiopaque barium to latex yields ideal contrast for imaging while preventing perfusion through capillary beds by maintaining the high viscosity of latex (Sedlmayr and Witmer, 2002). The volume of latex injected was approximately 12 mL, with perfusion continuing until latex emerged from the contralateral (non-intubated) common carotid artery (O'Brien and Williams, 2014). Acetic acid (10% glacial acetic acid solution [CH_3COOH]) was used to stop any minor latex leaks through severed muscular arteries, as acetic acid immediately sets latex. The venous system is not relevant to this study, and was not injected.

Following injection, the specimen was CT scanned at O'Bleness Memorial Hospital in Athens, Ohio, on a Toshiba Aquilion 64 slice CT scanner at 0.7 mm slice thickness. This resulted in an initial voxel size of $0.781 \times 0.781 \times 0.3\ mm^3$. The resulting image data were imported into Avizo (version 7.0; FEI Visualization Sciences Group, Burlington, MA). To ease handling of the data, the specimen was cropped to eliminate unusable data (*e.g.* air, packing material). Scan data were up-sampled to yield a voxel size of $0.5 \times 0.5 \times 0.5\ mm^3$. Up-sampling artificially adds voxels to the image data, a process which does not affect the inherent quality of the data. The result is a visually smoother digital surface. The carotid rete of the goat was segmented first by isolating distinctive gray-scale values, then manually inspected and edited to verify accuracy. The segmented arteries of interest were then rendered in 3-D (Fig. 2).

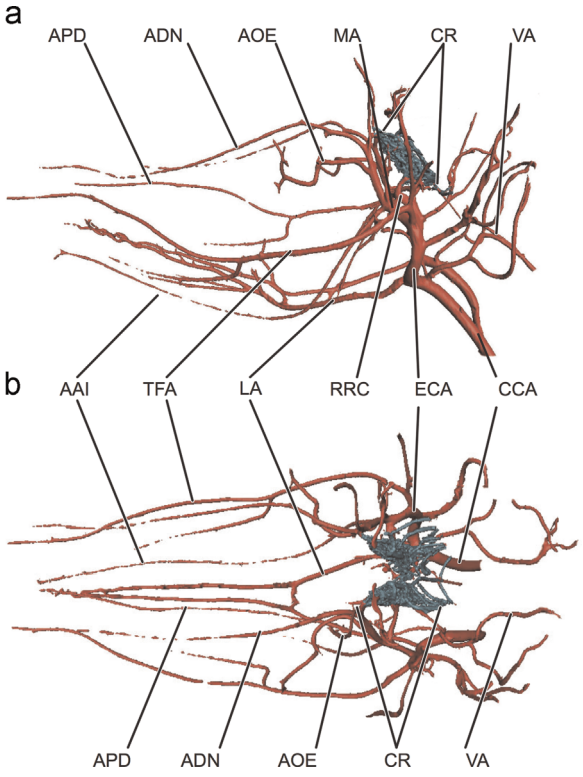

Fig. 2. Digital vascular model of the domestic goat (Capra hircus) generated for this study; (a) in lateral and (b) superior views. The carotid rete (CR, in teal) used to model CR hemodynamics is presented *in situ*. Abbreviations: AAI; ADN, anterior dorsal nasal artery; AOE; APD; CCA, common carotid artery; CR, carotid rete; ECA, external carotid artery; FA, facial artery; ICA, internal carotid artery; LA, lingual artery; MA, maxillary artery; RRC, rami ad rete caroticum; STA, superficial temporal artery; TFA, transverse facial artery; VA, vertebral artery.

2.2. Basic physical model

To ascertain a base-line expectation of the carotid rete's influence on hemodynamics and cerebral perfusion, changes in blood pressure along a length of artery were first calculated using basic mechanical equations describing fluid flow, including the Hagen–Poiseuille equation for incompressible fluids. The fundamental description of fluid flow through the vascular system can be described using the following equation:

$$Q = \frac{\Delta P}{R} \tag{1}$$

Flow rate (Q) depends on the pressure gradient, or driving pressure (ΔP), divided by the vascular resistance (R). Vascular resistance is dependent on a variety of factors that can be represented by the following equation:

$$R = \frac{8\mu L}{\pi r^4} \tag{2}$$

where L is the length of the vessel, μ is the dynamic viscosity, π is the mathematical constant, and r^4 is the vessel radius. The relationships between resistance, length, and radius are vital to the understanding of how blood flows through vessels of different dimensions. Resistance is directly proportional to vessel length, so a vessel that is twice the length of another vessel with the same radius will have twice the resistance to flow. More importantly, resistance is inversely proportional to the radius of the vessel raised to the fourth power, so a decrease in radius results in a substantial increase in resistance. For example, a relatively small,

two-fold decrease in radius results in a sixteen-fold increase in resistance. When combined these two equations produce the Hagen–Poiseuille equation for incompressible fluids.

$$Q = \frac{\Delta P \pi r^4}{8\mu L} \tag{3}$$

Hagen–Poiseuille's equation accounts for the fact that pressure and linear velocity are not constant along the length of a tube, but are highly sensitive to changes in blood vessel diameter, or radius as shown above. Small increases or decreases in blood vessel size greatly alter resistance to fluid movement, requiring concomitant changes in pressure to maintain the same flow rate. Hagen–Poiseuille's equation is considered a more accurate descriptor of circulatory flow as compared to other pressure, flow equations such as Bernoulli's equation (Vogel, 1994). For cardiovascular flow, Hagen–Poiseuille's equation may be simplified as follows:

$$Q \propto \frac{\Delta P \cdot r^4}{\mu \cdot L} \tag{4}$$

It is important to note that blood flow does not conform, *in vivo*, to all of the assumptions made by Hagen–Poiseuille's equation, such as rigid pipes, long distances from the pipe entrance, Newtonian fluids, and a laminar flow regime. Blood vessels are not rigid structures, but often have compliant walls. Many of the blood vessels in the rete run short distances and have large calibers, which pose a challenge to the formation of the parabolic profile, especially under high pulse rates. Importantly, Hagen–Poiseuille's equation assumes blood behaves as a Newtonian fluid. However, blood is a non-Newtonian fluid in which viscosity is neither constant nor independent of flow. Lastly, the pulsatile nature of blood flow means that it may not always flow under steady, laminar conditions. The results calculated using Hagen–Poiseuille's equation should be viewed as approximations of fluid behavior within arterial trees. Despite these caveats, the relationship described by Hagen–Poiseuille's equation is integral to the understanding of blood flow as it accurately describes the overwhelming influence of vessel radius on resistance, pressure, and flow rate. This utility of Hagen–Poiseuille's equation for describing blood flow has made it the predominant conceptual framework used by physicians to understand physiological and pathological changes in blood vessels (Klabunde, 2005; Westerhof et al., 2010).

To determine flow across the entire carotid rete, we first calculated the individual resistances of each retial segment using Eq. (2). However, this equation can only be applied to single vessels. Hagen–Poiseuille's equation is analogous with Ohm's law, so resistance calculated for individual vessels or segments of vessels can be modeled as an electrical circuit. In this analogy, vascular components can be conceptualized as individual wires within a complex network, and the overall resistance (R_{total}) of the arterial circuit can be calculated by modeling segments in series and/or parallel, as pertinent to the morphology of the vascular tree (Fig. 3). In a model for the carotid rete, the overall resistance is modeled as:

$$R_{Total} = R_{MA} + R_{CR} + R_{iICA} \tag{5}$$

The maxillary artery (MA) and intracranial segment of the internal carotid artery (iICA) are single, tubular vessels, so the resistance of each vessel (R_{MA} and R_{iICA}) can be calculated as a single value using Hagen – Poiseuille's equation (Fig. 3). Since the carotid rete is composed of numerous vessels, each accommodating flow in tandem, the resistance of the carotid rete (R_{CR}) should be considered as a parallel arrangement of resistances, with each small segment having a single resistance value calculated by Hagen–Poiseuille's equation (Fig. 3). The parallel circuit model was constructed by estimating the number and dimensions of segments within the carotid rete according to representative coronal and sagittal CT scan slices (Fig. 4). There were approximately 30 arterial cross sections in any given coronal slice (Fig. 4a), and sagittally, there were approximately three segments of small arteries (Fig. 4b). This approximated to 90 total segments of 100 μm average diameter (50 μm radius) and 150 μm average length. Since the meshwork was modeled after a parallel electronic circuit, the total resistance was calculated as:

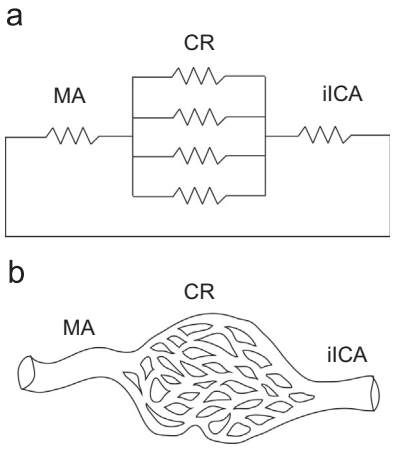

Fig. 3. Circuit diagram (a) and arterial tree schematic (b) for modeling the change in blood pressure resistance across the artiodactyl carotid rete (CR). In a simplified context, the hemodynamic changes within artiodactyl cranial arteries can be modeled with the maxillary artery (MA), carotid rete (CR), and intracranial internal carotid artery (iICA) analogous to an electrical circuit in series. The CR itself (center b) is modeled as a parallel circuit (center a).

$$R_{Parallel} = \frac{1}{\frac{1}{R_1} + \frac{1}{R_2} + \frac{1}{R_3} + \frac{1}{R_4} + \ldots + \frac{1}{R_n}} \tag{6}$$

where subscripts denote each individual vascular segment. For the rete model, $n = 90$.

2.3. Computational fluid dynamics model

2.3.1. Pre-processing

Following the methods of Bourke et al. (2014) for fluid flow through airway models, the 3D surface generations from Avizo were imported into Geomagic Studio (3D Systems Geomagic, Rock Hill, SC) to remove artifacts of segmentation and prepare the model for volumetric meshing. Skewed triangles were smoothed and refined until geometric congruence was reached across the surface. Gaps, holes, and intersections were all repaired in the model prior to export. The final surface model was approximately 800,000 triangles. As the rete is bilaterally symmetric, only one half was modeled to economize computational time.

The cleaned surface model was imported into the mesh generation software ICEM CFD (ANSYS Inc., Canonsburg, PA) for volumetric meshing. A tetrahedral–hexahedral hybrid mesh was created for the model. The tetrahedral mesh was created from the unstructured grid using the robust OCTREE method (Yerry and Sherphard, 1984). After mesh generation, the core of the mesh was removed and flooded with hexahedra. This hybrid mesh takes advantage of the many automated solutions available for tetrahedral meshing of unstructured grids (*e.g.*, Löhner and Parikh, 1988; Georges et al., 1988; Shephard and Georges, 1991) while providing the computational advantages associated with hexahedral meshes (Biswas and Strawn, 1998). The model was assigned a series of boundary conditions that would induce physiologically realistic flow through the rete. Inputs consisted of two pressure inlets located at the base of the maxillary arteries and a pressure outlet located at the segmented intracranial portion of the internal carotid artery (iICA), significantly downstream from the rete.

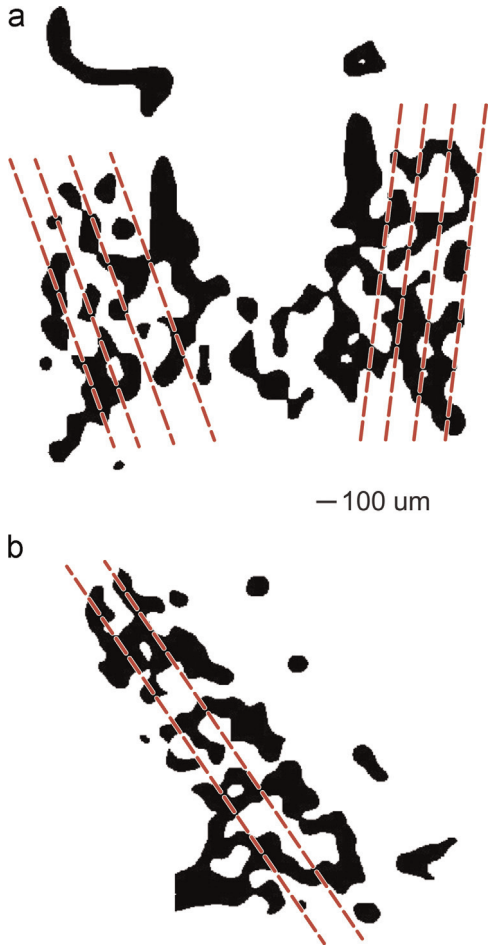

Fig. 4. Estimation of carotid rete metrics based on coronal (a) and sagittal (b) CT-scan slices. Lines (red dashes) indicate approximate partitions between coronal and sagittal segments. Retial segments had an average diameter of 100 μm.

Finally, an impermeable wall boundary was placed across the rete based of the connecting blood vessels. The placement of the inlets and outlet, coupled with the wall boundary on the rest of the model, ensured that blood could only flow from the maxillary arteries—through the rete—to the iICA, as it does in living artiodactyls. Downstream placement of the pressure outlet ensured that fluid flow artifacts caused by the modeling methodology would not affect the pertinent part of the model (*i.e.*, the rete). The wall boundary incorporated a standard 'no-slip' condition, meaning that there was no fluid movement at the wall-fluid boundary. This completed model consisted of 927,143 cells.

2.3.2. CFD assumptions

The rete model was imported into the fluid dynamics program Fluent (ANSYS Inc., Canonsburg, PA) where a finite-volume-based computational fluid dynamic analysis was performed. For most analyses a laminar viscosity model was chosen based on estimated flow rates and cross sectional data. This assumption agreed well with previous observations of laminarity in the circulatory system of animals (Vogel, 1994). Blood was given density and viscosity values that reflected empirically derived values obtained from similar sized goats (Alborch et al., 1977). We performed a steady-state analysis on the rete model under the assumption that blood acted as a Newtonian fluid. Although blood flow is pulsatile and non-Newtonian, a multitude of previous hemodynamic CFD analyses have found that gross blood flow patterns and wall shear stress (WSS) values remain practically identical under both steady-state, and transient analyses (Myers et al., 2001; Feldman et al., 2002; Johnston et al., 2004, 2005). Similarly, although it is possible to model blood as a non-Newtonian fluid, the computational expenses largely outweigh the increase in resolution (Johnston et al., 2005). Various studies have investigated the difference between modeling blood viscosity as Newtonian versus non-Newtonian, and have found small or insignificant differences between the two modeling approaches (Cebral et al., 2005; Johnston et al., 2005; Valencia et al., 2006; Utter and Rossmann, 2007; Fisher and Rossmann, 2009; Radaelli et al., 2008; Morales et al., 2011, 2013).

2.3.3. CFD processing

We analyzed the CFD rete model under a variety of scenarios. Using empirically collected data on captive goats (from Alborch et al., 1977), we analyzed blood flow through the rete during the pressure peak and nadir of the cardiac cycle (*i.e.*, ventricular systole and diastole). High and low pressure values were placed on the pressure inlets (branches of the maxillary artery), whereas the pressure outlet was allowed to vary in response to the mass of flow passing through it using the 'target-mass-flow-rate' option in Fluent. Mass flow was obtained using the following equation:

$$MF = \rho_B * Q_B \tag{7}$$

where MF is the mass flow, ρ_B is the density of blood (1.06 kg/L) and Q_B is the volumetric flow rate of blood ($2.08e^{-3}$ L/s).

Along with the systolic and diastolic phases of the cardiac cycle, we further tested the stability of the rete by modeling the extremely hypertensive flow rates experienced by giraffes under natural, head-lowered posture. Under this condition, cerebral blood pressure is an average of 2.36 times higher than systolic blood pressure (direct measurements by van Citters et al. (1968), with further estimates from Patterson et al. (1957), van Citters et al. (1969), Mitchell and Skinner (1993) and Mitchell et al. (2008)), with concomitantly higher blood flow rates. The goat rete digitized for this study is morphologically similar to that of the giraffe (Lawrence and Rewell, 1948; Daniel et al., 1953; Carlton and McKean, 1977), albeit substantially smaller. To investigate giraffe-like hypertension using our pre-existing rete model, we multiplied the mean arterial pressure of the goat by a scaling factor of 2.36. Note that Eq. (3) indicates that a linear relationship exists between pressure change and flow rate. Thus, if we increase the pressure at our inlets—the branches of the maxillary artery—the volumetric flow rate must increase as well. This pressure-flow relationship has been documented in giraffes, where authors observed that a doubling of blood pressure while recumbent caused a doubling of blood flow through the carotid artery (van Citters et al., 1968). Thus, to compensate for the increased pressure in our goat model, we increased the flow rate by the same scaling factor (Table 1).

Cross sectional analysis of the maxillary arterial inputs and the iICA output revealed low Reynolds numbers in both vessels (38–167), suggesting that blood flow remained laminar even under these high flow rates. Regardless, due to the much higher flow rate in the hypertensive model, we tested it using both the standard laminar viscosity model and the Wilcox two equation κ–ω turbulence model. For the latter we incorporated a shear stress transport equation to account for transitional flows (Chen et al., 2009), and a low Reynolds number correction was added to the model to account for the rather low values recorded from the vessel cross sections. This more complicated model takes into account turbulence found both in the center of the flow stream as well as near the wall boundary. Though more computationally intensive, this model has the capacity to capture flow patterns that would be missed under a laminar viscosity model.

Models ran until the results obtained from each analysis had reached a specified level of stability and consistency, referred to as convergence (Tu et al., 2013). This indicated that the numerical

Table 1
Flow parameters for goat CFD model.

Flow parameters	Systole	Diastole	Hypertension
Pressure (mmHg)	100.61	58.18	236
Flow rate (mL/s)	2.08	2.08	4.91

process used to solve the problem had asymptotically approached the "true" solution (*i.e.*, blood flow through an actual carotid rete) given the conditions provided. In CFD, convergence is determined in one of two ways. The first method looks at the global imbalances in the values for each node within the mesh between steps, or iterations, of the model. Imbalances, or errors, between each iteration are referred to as residuals (Tu et al., 2013). The smaller these residuals are the smaller the error is and the more converged the solution becomes. Our study monitored momentum, pressure and continuity (conservation of fluid mass). These three variables are generally considered solved when their residuals have fallen below 1×10^{-3} (Tu et al., 2013). However, for this physiological study, we applied the slightly stricter criterion of 1×10^{-4} (Craven et al., 2009; Bourke et al., 2014). The second means of determining convergence is to directly monitor the variables in question. We did this by using surfaces designed to output data from a single location only (point surfaces). Multiple point surfaces were placed along the rete model to monitor velocity and pressure values. The presence of the same value on these surfaces across multiple iterations of the model indicated stability of the solution, letting us know that the model had converged.

2.3.4. Mesh independence

Obtaining mesh independent results is important to any CFD study, as the resolution of the mesh can greatly affect the results and interpretations of an analysis. Previous CFD studies of hemodynamics have found that a relatively coarse grid is capable of accurately capturing velocity profiles and other general aspects of the flow field (Prakesh and Ethier, 2000). Our initial mesh, consisting of 927,143 cells, was fairly high resolution for the purpose of this study. However, to ensure mesh independent results, we performed a solution-based adaptive mesh refinement (AMR). This process used data from a fairly converged solution to determine regions of the mesh where cell count was too low to accurately resolve the flow field. These regions were marked and refined by the program. The newly refined model was run under the same criteria as the original mesh, and the results were compared to each other. This process was repeated until meshes returned values that were approximately equal (falling below a predetermined margin of error), at which point they were considered to be mesh independent. AMR of our rete mesh resulted in a modest increase in mesh resolution to 1,069,907 cells, with reported values of interest (*i.e.*, pressure) between this refined model and the original model differing by less than 1% (Fig. 5).

2.3.5. Post-processing

Successfully converged models were input into the CFD module of Avizo (Avizo Wind) where data were visualized, quantified, and interpreted. Identical regions of interest (ROI) were placed on the different rete models. These ROI were used to obtain the average pressure drop across the rete under each individual scenario. Cross sections taken normal to the flow field were used to calculate flow rate through branches of the rete by integrating mean flow velocity across the cell faces within each cross section before converting to volumetric flow.

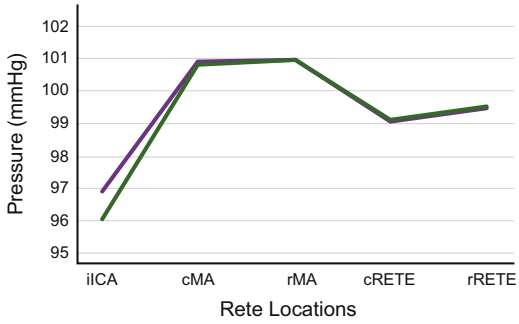

Fig. 5. Graph showing convergence of results between 927,143 cell model (green) and a 1,069,907 cell model (purple). The largest divergence was observed near the inlets and outlets (difference of ~1%). In contrast data from within the rete were extremely similar (difference of ~0.1%).

3. Results

3.1. Basic model results

With $\mu=2.42\times10^{-3}$ kg/m s as the viscosity of blood at 37 °C, the resistance of each individual retial segment was equal to:

$$R\propto\frac{2.42\times10^{-3}\cdot150}{50^4}=5.808\times10^{-8}\ \text{kg/m}^4\ \text{s}$$

In the case of the carotid rete, there were approximately 90 segments, each of similar size and therefore similar resistance. The total resistance of the rete meshwork, in parallel, was:

$$R_{rete}=\frac{1}{\left(90\left(\frac{1}{5.808\times10^{-8}}\right)\right)}=6.4533\times10^{-10}\ \text{kg/m}^4\ \text{s}$$

If this value were to be added, in series, from the blood pressure of a simple tubular artery, such as the maxillary artery or the internal carotid artery, the additional resistance of the rete is negligible. Mean arterial pressure measured in the internal maxillary artery of a goat was approximately 97 mmHg (Alborch et al., 1977), so it is expected that blood pressure at the beginning of the intracranial internal carotid artery would likewise be near 97 mmHg.

3.2. CFD model results

Under all models analyzed, the majority of pressure drop was localized to the base of the iICA, indicating that the highly convoluted, mesh-like rete contributed very little intrinsic pressure loss. Extreme decreases in pressure at the distal iICA were a consequence of having to model flow through the rete as an open system. In reality, the iICA belongs to a closed system, contributing to the cerebral arterial circle and major cerebral vessels.

Pressure drop at each ROI was less than 2% of the input arterial pressure. Under diastolic and systolic pressures, the average pressure across the rete was nearly identical to the pressure of the incurrent blood, dropping by only 1.3 and 1.8 mmHg, respectively (Fig. 6; Table 2). Across the hypertensive model, comparison of gross flow patterns and pressure changes revealed nearly identical flow patterns between the laminar viscosity and turbulence models (Fig. 7). This indicated that, under the flow assumptions used for this analysis, blood flow through the rete remained laminar across a wide variety of pressures. Compared to the systolic and diastolic simulations, the hypertensive model, with its concomitantly higher flow rate, calculated a larger absolute drop in pressure (5.4 mmHg, Table 2). However, the relative decrease across the rete was equivocal (less than 2%).

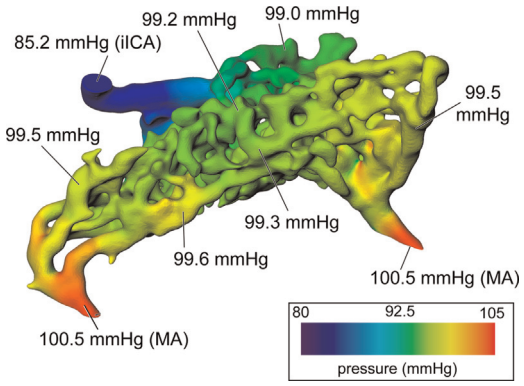

Fig. 6. Blood pressure change throughout the carotid rete during the systolic phase of the cardiac cycle. Warm colors represent higher pressure and cool colors represent lower pressure. The extreme drop in pressure at the intracranial internal carotid artery (iICA) is a consequence of modeling the output of the rete as an open system and does not reflect biological reality. Pressure at the maxillary artery (MA) model inlets is 100.5 mmHg. Where the retial segments recondense to form the iICA, pressure drops to 99.2 mmHg, a difference of 1.3 mmHg (or a 1.2% reduction in pressure).

Table 2
Pressure results (mmHg) from CFD analyses.

Mean pressure values	Systole	Diastole	Hypertension
Maxillary branches	100.5	57.7	233.4
Carotid Rete	99.2	56.4	228.0
Intracranial ICA	85.2	42.7	161.1

General flow patterns in all goat models were similar, with blood entering from the branches of the maxillary artery and quickly spreading across the rete prior to anastomosing at the base of the iICA (Fig. 7). Despite the myriad of branches present in the rete model, blood channels were never observed coalescing to form turbulent eddies. Secondary flows were limited to a small number of dorsal retial branches that fed directly into the iICA. Flow rate and concentration were high at the model outlet (iICA), and inlets (maxillary arteries). Within the retial segments, the distribution of flow was diffuse and meandering (Fig. 8). Flow rates of approximately 0.16 mL/s were documented through many of the individual retial branches during systole, however significant variation was observed among the branches with more distal portions of the rete showing slower flow (Fig. 8).

4. Discussion

The negligible increase in vascular resistance calculated by both the simple and CFD models suggests that the mesh-like structure of the carotid rete is unlikely to play a role in regulating cerebral perfusion and blood pressure. In this respect, the function of the carotid rete is analogous to the function of the tubular internal carotid artery possessed by most other mammals. This may seem counter-intuitive, but with careful consideration of fluid flowing through parallel, segmental vessels, these results are not so surprising. Resistance in a parallel circuit is calculated as the residual of each segmental fraction of resistance, so addition of more segments further reduces the change in total resistance across the network. In a network with as many segments as the artiodactyl carotid rete, the added value of resistance quickly approaches zero, rendering the structure as a whole equivocal to a single, tubular artery. More complex elements that are inherent to the carotid rete, such as multiple, non-parallel branches, minor secondary flows, and increased wall surface areas (which increase wall shear stress), add only a small amount of resistance in CFD models. The result is a non-zero, but inconsequential drop in blood pressure (1.3–1.6 mmHg—approximately 1% of incurrent blood pressure). Moreover, the models revealed variably diffuse and reduced flow rates. Although these varying flow rates did not result in a significant change in blood pressure, this diffusion and reduction in velocity would be highly advantageous for heat exchange.

Even though these results are physically sound, are they biologically relevant? The structural properties of arterial wall morphology and vascular physiology may also impact the function of the carotid rete. The histology of the carotid rete of the sheep (*Ovis aries*), as investigated by Khamas et al. (1983), illustrated a strikingly different arterial and venous wall composition when compared to distributing arteries of similar diameter. The carotid rete itself is composed of segments approximately 100 μm in diameter. This lumen diameter is typical of vessels classified as "large arterioles". For arteries of this caliber, the three layers of the arterial wall (tunica intima, media, and adventitia) are relatively thin: the tunica intima consists of a single layer of squamous epithelium; the tunica media is comprised by fewer than 10 concentric layers of smooth muscle cells; and the tunica adventitia is usually the same width as the media. The arterial branches of the carotid rete, on the other hand, are characteristic of muscular arteries, although the thickness and orientation of smooth muscle cells in the tunica media is variable depending on proximity to proximal and distal distributing arteries. The thin tunica intima displays a well-developed internal elastic lamina, while the fibrous tunica adventitia lacks a consistent external elastic lamina. There are a large number of epithelioid cells in the walls of carotid rete arteries. Upon unification of the carotid rete into a small, intracranial internal carotid artery, the tunica media thickens by doubling the layers of circularly arranged smooth muscle cells. The tunica adventitia is also thickened, and contains a multitude of vasa and nervi vasorum. The arrangement of smooth muscle cells in the walls of the carotid rete arteries suggests that, upon stimulation, the rete contracts in three dimensions. This would result in a decrease in lumen diameter as well as blood vessel length. The presence of a distinct tunica intima with a continuous internal elastic membrane serves as a barrier to the exchange of metabolites, macromolecules, and fluids between the arterial carotid rete and the cavernous sinus (although see Grzegorzewski et al. (1995, 1997), for exceptions in suiform artiodactyls). The endothelium may also supply the smooth muscle with important vasodilatory substances such as nitric oxide (NO) and prostacyclin (PGI_2) (Klabunde, 2005).

In a sympathetic context, the carotid rete is not contractile. A number of *in vivo* studies have quantified the impact of adrenergic stimulants on maxillary, retial, and intracranial arteries (Dieguez et al., 1983, 1987, 1988; Lluch et al., 1984). These analyses indicate that the rete itself may not be responsive to sympathetic stimulation. In these studies, cranial arteries were dissected from goats and subdivided based on vessel diameter: two groups of retial arteries (150–250 μm; 300–500 μm), and proximal and distal cerebral arteries (all between 300 and 500 μm), were pinned to force transducers. Contractile response was measured across electrical stimulation and tyramine, vasopressin, and norepinephrine application. Measured forces were trivial in retial segments, but significant in cerebral arteries. These results imply that there are few sympathetic nerve endings and a paucity of catecholamine receptors in the arterial walls of the carotid rete itself. In artiodactyls, the result of sympathetic activity on intracranial blood flow is nearly identical to that of mammals with an ICA (Dieguez et al., 1983, 1987, 1988; Lluch et al., 1984), however, altered resistance is due to contraction of the cerebral arteries alone. Another mechanism for control of cerebral blood pressure is the presence of baroreceptor cells in the carotid sinus. These receptors are stimulated by changes in arterial pressure, initiating a reflex arc that modulates sympathetic and vagal parasympathetic innervation of the heart. When

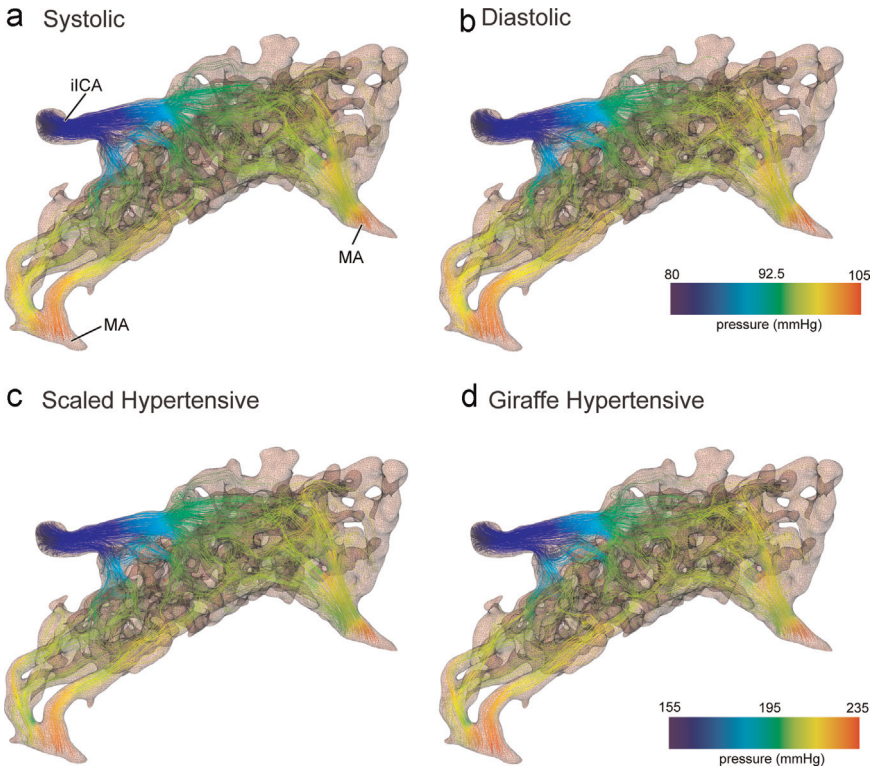

Fig. 7. Blood pressure distribution throughout the rete under (a) systolic, (b) diastolic, (c) scaled (laminar) hypertensive, and (d) giraffe (turbulent) hypertensive. Warm colors represent higher pressure and cool colors represent lower pressure. Note differences in pressure scale bars: (a and b) range from 80 to 105 mmHg, whereas (c and d) range from 165 to 235 mmHg. The magnitude of blood pressure change is similar across each scenario, with each model calculating a decrease of 2% or less.

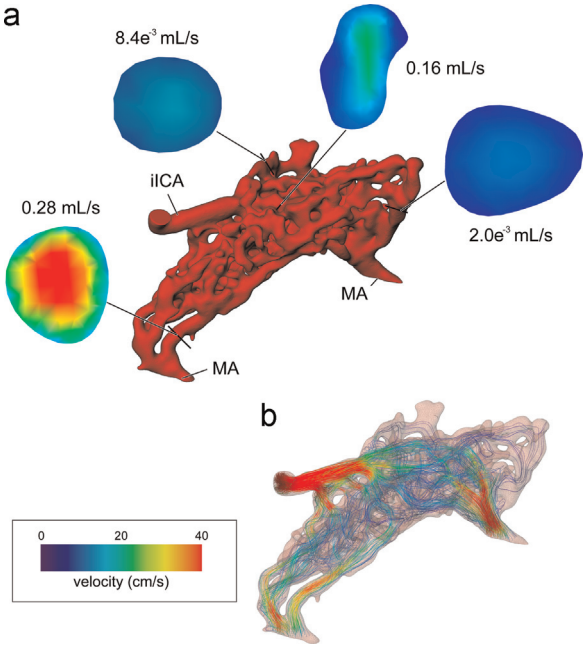

Fig. 8. Cross-sectional flow rates taken normal to the direction of flow at regions of interest within the rete (a), and flow distribution throughout the carotid rete in its entirety (b). Flow rate is highest at the model inputs and outlet, and greatly decreased within retial segments. Warm colors represent higher flow velocities and cool colors represent lower flow velocities.

the pressure inside the artery increases, the firing rate of integrated pressoceptors increases, and *vise versa* upon decreased pressure. Under normal blood pressure conditions, carotid body receptor firing helps maintain tonic parasympathetic stimulation of the heart rate. In response to a high pulse pressure or mean blood pressure, efferent signals from the carotid body stimulate the nucleus tractus solitarius of the central nervous system to decrease sympathetic activity and increase parasympathetic influence of the heart rate (Klabunde, 2005). The normal location for these cells is at the bifurcation of the internal and external carotid arteries. Artiodactyls, by lacking an internal carotid artery altogether, also lack such a bifurcation. It is not necessarily expected that the carotid body would be absent from the extracranial carotid artery, or replicated distal to the carotid rete. Intriguingly, the tunica adventitia of the intracranial internal carotid artery contains such baroreceptor cells. Khamas et al. (1983) postulate that these carotid body cells migrate to the internal carotid artery upon embryonic disintegration of the extracranial internal carotid artery. The location of these receptors downstream to the carotid rete means that blood pressure and heart rate are regulated *after* blood has passed through the rete.

The histology and physiology of the carotid rete and its surrounding vessels, much like the physical and computational models generated for this study, indicate that the carotid rete has few, if any, mechanical or physiological mechanisms to respond to changes in blood pressure. Its relatively stiff, but largely non-contractile arterial walls are unlikely to passively contract or expand across rapid increases or decreases in blood pressure. The lack of response to vasoactive substances, and the downstream location of baroreceptors (normally situated extracranially) also separate the carotid rete from a role in cranial blood pressure regulation. Based on this evidence, we endorse alternative explanations for regulation of cerebral blood pressure in artiodactyls, such as diversion of cerebral blood flow to the jugular veins or non-collapsible vertebral venous plexus (Seymour and Johansen, 1987; Seymour et al., 1993; Hicks and Munis, 2005; Mitchell et al., 2008), or a shunting of blood away from the cranial cavity *via* a

large, arterial occipito-verterbral anastomosis (Lawrence and Rewell, 1948; Mitchell and Skinner, 1993).

Acknowledgments

We thank the Ohio University Student Enhancement Award & Graduate Student Senate Original Work Grants (HDO & JB), the American Society of Mammalogists Grants-In-Aid program (HDO), the Society for Integrative and Comparative Biology Grants-In-Aid program (HDO), and fellowships from the Ohio Center for Ecology and Evolutionary Studies (HDO) and the National Science Foundation Graduate Research Fellowship (JB), for funding this research. S.H. Williams loaned the specimen of *Capra* used in this study, and L.M. Witmer and H. Skinner-Rockhold conducted CT scanning at O'Bleness Memorial Hospital in Athens, Ohio. We thank Dr. Denise Kirschner and an anonymous reviewer, as well as N.J. Stevens, R.E. Klabunde, and P.M. Gignac for helpful comments on the manuscript.

References

Aas-Hansen, O., Folkow, L.P., Blix, A.S., 2000. Panting in reindeer (*Rangifer tarandus*). Am. J. Physiol.-Reg. I 279, R1190–R1195.
Alborch, E., Gomez, B., Dieguez, G., Marin, J., Lluch, S., 1977. Cerebral blood flow and vascular reactivity after removal of the superior cervical sympathetic ganglion in the goat. Circ. Res. 41, 278–282.
Ask-Upmark, E., 1935. The carotid sinus and the cerebral circulation. An anatomical, experimental and clinical investigation, including some observations on rete mirabile caroticum. Acta Psychiatr. (Kbh.) 6 (Suppl), S1–S374.
Baker, M.A., Hayward, J.N., 1967. Carotid rete and brain temperature of cat. Nature 216, 139–141.
Biswas, R., Strawn, R.C., 1998. Tetrahedral and hexahedral mesh adaptation for CFD problems. App. Numer. Math. 26, 135–151.
Bourke, J.M., Porter, Wm. R., Ridgely, R.C., Lyson, T.R., Schachner, E.R., Bell, P.R., Witmer, L.M., 2014. Breathing life into dinosaurs: tackling challenges of soft-tissue reconstruction and nasal airflow in extinct species. Anat. Rec. 297, 2148–2186.
Carlton, C., McKean, T., 1977. The carotid and orbital retia of the pronghorn, deer, and elk. Anat. Rec. 189, 91–108.
Caputa, M., 2004. Selective brain cooling: a multiple regulatory mechanism. J. Therm. Biol. 29, 691–702.
Cebral, J.R., Castro, M.A., Appanaboyina, S., Putman, C.M., Millan, D., Frangi, A.F., 2005. Efficient pipeline for image-based patient-specific analysis of cerebral aneurysm hemodynamics: technique and sensitivity. IEEE Trans. Med. Imaging 24, 457–467.
Chen, X.B.B.E., Lee, P.H., Chong, V.F.H., Wang, D.Y., 2009. Assessment of septal deviation effects on nasal air flow: a computational fluid dynamics model. Laryngoscope 119, 1730–1736.
Craven, B.A., Paterson, E.G., Settles, G.S., Lawson, M.J., 2009. Development and verification of a high-fidelity computational fluid dynamics model of canine nasal airflow. J. Biomech. Eng. 131, 91002-1–91002-11.
Daniel, P.M., Dawes, J.D., Pritchard, M.M., 1953. Studies of the carotid rete and its associated arteries. Philos. Trans. R. Soc. B 237, 173–208.
Dieguez, G., Conde, M.V., Gomez, B., Iglesias, J.R., Marin, J., Lluch, S., 1983. Rete mirabile of goat: in vitro effects of adrenergic stimulation. Brain Res. 289, 281–284.
Dieguez, G., Garcia, A.L., Conde, M.V., Gomez, B., Santamaria, L., Lluch, S., 1987. In vitro studies of the carotid rete mirabile of Artiodactyla. Microvasc. Res. 33, 143–154.
Dieguez, G., Garcia-Villalon, A.L., Gomez, B., Lluch, S., 1988. Hemodynamic significance of the carotid rete during changes in arterial blood pressure. Am. J. Physiol. 254 (5 Pt. 2), 770–775.
Edelman, N.H., Epstein, N.S., Cherniak, N., Fisher, A.P., 1972. Control of cerebral blood flow in the goat: role of the carotid rete. Am. J. Physiol. 223, 615–619.
Feldman, C.L., Ilegbusi, O.J., Hu, Z., Nesto, R., Waxman, S., Stone, P.H., 2002. Determination of in vivo velocity and endothelial shear stress patterns with phasic flow in human coronary arteries: a methodology to predict progression of coronary atherosclerosis. Am. Heart J. 143, 931–939.
Fisher, C., Rossmann, J.S., 2009. Effect of non-Newtonian behavior on hemodynamics of cerebral aneurysms. J. Biomech. Eng. 131, 091004.
Fuller, A., Moss, D.G., Skinner, J.D., Jessen, P.T., Mitchell, G., Mitchell, D., 1999. Brain, abdominal and arterial blood temperatures of free-ranging eland in their natural habitat. Pflüg. Arch. 438, 671–680.
Georges, P., Hecht, F., Saltel, E., 1988. Constraint of the boundary and automatic mesh generation. In: Sengupta, S., Håuser, J., Eiseman, P.R., Thompson, J.F. (Eds.), Numerical Grid Generation in Computational Fluid Mechanics. Pineridge, Swansea, UK.
Gillilan, L.A., 1974. Blood supply to brains of ungulates with and without a rete mirabile caroticum. J. Comput. Neurosci. 153 (3), 275–290.
Goetz, R.H., 1955. Preliminary observations on the circulation of the giraffe. Trans. Am. Coll. Cardiol. 5, 39–48.
Grzegorzewski, W.J., Skipor, J., Wasowska, B., Krzymowski, T., 1995. Counter current transfer of oxytocin from the venous blood of the perihypophyseal cavernous sinus to the arterial blood of the carotid rete supplying the hypophysis and brain depends on the phase of the estrous cycle in pigs. Biol. Reprod. 52, 139–144.
Grzegorzewski, W.J., Skipor, J., Wasowska, B., Krzymowski, T., 1997. Countercurrent transfer of ^{125}I-LHRH in the perihypophyseal cavernous sinus-carotid rete vascular complex, demonstrated on isolated pig heads perfused with autologous blood. Domest. Anim. Endocrinol. 14, 149–160.
Hayward, J.N., Baker, M.A., 1969. A comparative study of the role of cerebral arterial blood in the regulation of brain temperature in five mammals. Brain Res. 16, 417–440.
Hargens, A.R., Millard, R.W., Petterson, K., van Hoven, W., Gershuni, D.H., Johansen, K., 1987. Transcapillary fluid balance in giraffe. Adv. Microcirc. 13, 195–202.
Hicks, J.W., Munis., J.R., 2005. The siphon controversy: an integration of concepts and the brain as a baffle. Am. J. Physiol. 289, R627–632.
Janis, C.M., 1976. The evolutionary strategy of the Equidae and the origins of rumen and cecal digestion. Evolution 30, 757–774.
Janis, C.M., 1989. A climatic explanation for patterns of evolutionary diversity in ungulate mammals. Palaeontology 32, 463–481.
Janis, C.M., 2007. Artiodactyl paleoecology and evolutionary trends. In: Prothero, D. R., Foss, S.E. (Eds.), The Evolution of Artiodactyls. Johns Hopkins University Press, Baltimore, pp. 292–302.
Janis, C.M., 2008. An evolutionary history of browsing and grazing ungulates. In: Gordon, I.J., Prins, H.H.T. (Eds.), The Ecology of Browsing and Grazing: Ecological Studies. Springer, New York, pp. 21–45.
Janis, C.M., Scott, K.M., Jacobs, L.L., 1998. Evolution of tertiary mammals of North America. Cambridge University Press, Cambridge.
Jernvall, J., Hunter, J.P., Fortelius, M., 1996. Molar tooth diversity, disparity, and ecology in Cenozoic ungulate radiations. Science 274, 1489–1492.
Jessen, C., 1998. Brain cooling: an economy mode of temperature regulation in artiodactyls. News Physiol. Sci. 13, 281–286.
Jessen, C., Laburn, H.P., Knight, M.H., Kuhnen, G., Goelst, K., Mitchell, D., 1994. Blood and brain temperatures in free-ranging black wildebeest in their natural environment. Am. J. Physiol. 267, R1528–R1536.
Johnston, B.M., Johnston, P.R., Corney, S., Kilpatrick, D., 2004. Non-Newtonian blood flow in human right coronary arteries: steady state simulations. J. Biomech. 37 (5), 709–720.
Johnston, B.M., Johnston, P.R., Corney, S., Kilpatrick, D., 2005. Non-Newtonian blood flow in human right coronary arteries: transient simulations. J. Biomech. 39, 1116–1128.
Kanagasuntheram, R., Krishnamurti, A., 1965. Observations on the carotid rete in the lesser bush baby (Galago senegalensis senegalensis). J. Anat. 99 (4), 861–875.
Kohler, M., 1993. Skeleton and habitat of recent and fossil ruminants. Münch. Geowiss. Abh. A Geol. Paläontol 25, 1–88.
Kohler, M., Moya-Sola, S., 2001. Phalangeal adaptations in the fossil insular goat Myotragus. J. Vertibr. Paleontol. 21 (3), 621–624.
Khamas, W.A., Goshal, N.G., Bal, H.S., 1983. Histomorphologic structure of the carotid rete-cavernous sinus complex and its functional importance in sheep (*Ovis aries*). Am. J. Vet. Res. 45 (1), 156–158.
Klabunde, R.E., 2005. Cardiovascular Physiology Concepts. Lippincott Williams and Wilkins, Baltimore, MD.
Kuhnen, G., 1997. Selective brain cooling reduces respiratory water loss during heat stress. Comp. Biochem. Pysiol. A 118, 891–895.
Lawrence, W.E., Rewell, R.E., 1948. The cerebral blood supply in the Giraffidae. Proc. Zool. Soc. (London) 118, 202–212.
Lluch, S., Conde, M.V., Dieguez, G., Lopez de Pablo, A.L., Gonzalez, M.C., Estrada, C., Gomez, B., 1984. Evidence for the direct effect of vasopressin on human and goat cerebral arteries. J. Pharmacol. Exp. Ther. 228 (3), 749–755.
Löhner, R., Parikh, P., 1988. Generation of three-dimensional unstructured grids by the advancing-front method. Int. J. Numer. Methods Fluids 8, 1135–1149.
Lust, A., Fuller, A., Maloney, S.K., Mitchell, D., Mitchell, G., 2007. Thermoregulation in pronghorn antelope (Antilocapra americana, Ord) in the summer. J. Exp. Biol. 210, 2444–2452.
Maloney, S.K., Fuller, A., Mitchell, G., Mitchell, D., 2002. Brain and arterial blood temperatures of free-ranging oryx (*Oryx gazella*). Pflug. Arch. 443, 437–445.
Myers, J.G., Moore, J.A., Ojha, M., Johnston, K.W., Ethier, C.R., 2001. Factors influencing blood flow patterns in the human right coronary artery. Ann. Biomed. Eng. 29, 109–120.
Miletich, D.J., Ivankovic, A.D., Albrecht, R.F., Toyooka, E.D., 1975. Cerebral hemodynamics following internal maxillary artery ligation in the goat. J. Appl. Physiol 38 (5), 942–945.
Mitchell, G., Lust, A., 2008. The carotid rete and artiodactyl success. Biol. Lett. 4, 415–418.
Mitchell, G., Skinner, J.D., 1993. How giraffe adapt to their extraordinary shape. Trans. R. Soc. (South Africa) 48, 207–218.
Mitchell, D., Laburn, H.P., Nijland, M.J.M., Zurovsky, Y., Mitchell, G., 1987. Selective brain cooling and survival. S. Afr. J. Sci. 83, 598–604.

Mitchell, G., Bobbitt, J.P., Devries, S., 2008. Cerebral perfusion pressure in giraffe: Modeling the effects of head-raising and -lowering. J. Theory Biol. 252, 98–108.
Moore, K.L., Dalley, A.F., Agur, A.M.R., 2010. Clinically Oriented Anatomy. Lippincott Williams & Wilkins, Baltimore, MD.
Morales, H.G., Kim, M., Vivas, E.E., Villa-Uriol, M.C., Larrabide, I., Sola, T., Guimaraens, L., Frangi, A.F., 2011. How do coil configuration and packing density influence intra-aneurysmal hemodynamics? Am. J. Neuroradiol. 32, 1935–1941.
Morales, H.G., Larrabide, I., Geers, A.G., Aguilar, M.L., Frangi, A.F., 2013. Newtonian and non-Newtonian blood flow in coiled cerebral aneurysms. J. Biomech. 46, 2158–2164.
Negus, V.E., 1958. The comparative anatomy and physiology of the nose and paranasal sinuses. Livingstone, London, England.
O'Brien, H.D., Williams, S.H., 2014. Using biplanar fluoroscopy to guide radiopaque vascular injections: a new method for vascular imaging. PLoS One 9 (5), e97940.
Patterson, J.L., Warren, J.V., Doyle, J.T., Gauer, O., Keen, E.N., Goetz, R.H., 1957. Circulation and respiration in the giraffe. J. Clin. Investig. 36, 919.
Prakesh, S., Ethier, C.R., 2000. Requirements for mesh resolution in 3D computational hemodynamics. J. Biomech. Eng. 123, 134–144.
Radaelli, A.G., Augsburger, L., Cebral, J.R., Ohta, M., Ru, D.A., Socci, L., Verhegghe, B., Frangi, A.F., 2008. Reproducibility of haemodynamical simulations in a subject-specific stented aneurysm model – a report on the virtual intracranial stenting challenge 2007. J. Biomech. 41, 2069–2081.
Robertshaw, D., 2006. Mechanisms for the control of respiratory evaporative heat loss in panting animals. J. Appl. Physiol. 101, 664–668.
Robertshaw, D., Demi'el, R., 1983. The effect of dehydration on the control of panting and sweating in the black Bedouin goat. Physiol. Zool. 56, 412–418.
Sedlmayr, J.C., Witmer, L.M., 2002. Rapid technique for imaging the blood vascular system using stereoangiography. Anat. Rec. 267, 330–336.
Seymour, R.S., Johansen, K., 1987. Blood flow up hill and downhill: does a siphon facilitate circulation above the heart. Comp. Biochem. Physiol. A 88, 167–170.
Seymour, R.S., Hargens, A.R., Pedley, T.J., 1993. The heart works against gravity. Am. J. Physiol. 265, R715–R720.
Shephard, M., Georges, M., 1991. Automatic three-dimensional mesh generation by the finite octree technique. Int. J. Numer. Methods Eng. 32, 709–749.
Shoshani, J., Kupsky, W.J., Marchant, G.H., 2006. Elephant brain Part I: gross morphology, functions, comparative anatomy, and evolution. Brain Res. Bull. 70, 124–157.
Sisson, S., Grossman, J.D., 1967. The Anatomy of the Domestic Animals, fourth ed. WB Saunders, Philadelphia and London.
Taylor, C.R., 1970. Dehydration and heat: effects on temperature regulation of East African ungulates. Am. J. Physiol. 219, 1136–1138.
Taylor, C.R., Lyman, C.P., 1972. Heat storage in running antelopes: independence of brain and body temperatures. Am. J. Physiol. 222, 114–117.
Tu, J., Yeoh, G.H., Liu, C., 2013. Computational Fluid Dynamics, Second Edition: A practical Approach. Butterworth-Heinemann, United Kingdom.
Utter, B., Rossmann, J.S., 2007. Numerical simulation of saccular aneurysm hemodynamics: influence of morphology on rupture risk. J. Biomech. 40, 2716–2722.
Valencia, A., Zarate, A., Galvez, M., Badilla, L., 2006. Non-Newtonian blood flow dynamics in a right internal carotid artery with a saccular aneurysm. Int. J. Numer. Method H 50, 751–764.
van Citters, R.L., Kemper, W.S., Franklin, D.L., 1968. Blood flow and pressure in the giraffe carotid artery. Comp. Biochem. Physiol. 24, 1035–1042.
van Citters, R.L., Franklin, D.L., Vatner, S.F., Patrick, T., Warren, J.V., 1969. Cerebral haemodynamics in the giraffe. Trans. Assoc. Am. Phys. 82, 239–304.
Vogel, S., 1994. Life in Moving Fluids, 2nd ed. Princeton University Press, Princeton, NJ.
Westerhof, N., Stergiopulos, N., Noble, M.I.M., 2010. Snapshots of Hemodynamics: an Aid for Clinical Research and Graduate Education. Springer, New York, NY, p. 272.
Wible, J.R., 1984. The Ontogeny and Phylogeny of the Mammalian Cranial Arterial Pattern. Ph.D. dissertation. Duke University, Durham, North Carolina.
Yerry, M., Sherphard, M., 1984. Automatic three-dimensional mesh generation by the modified-octree technique. Int. J. Numer. Methods Eng. 20, 1965–1990.